# Numerical Study of the Transition from Regular to Mach Reflection on Planar and Axisymmetric Reflection Surfaces



Marcel Grzeszczyk, J. J. Gottlieb, and C. P. T. Groth

Abstract The transition from regular to Mach reflection remains a key area of study for unsteady oblique shock interactions with a solid surface. In this study, high-fidelity computational fluid dynamics (CFD) based on the combination of an upwind finite-volume spatial discretization and an anisotropic block-based adaptive mesh refinement (AMR) procedure applied to the solution of the Euler equations governing compressible gaseous flows is used in conjunction with a systematic post-processing methodology to accurately compute and compare the regular-to-Mach reflection (RR-MR) transition on wedges, cylinders, cones, and spheres. The objective of this study is to determine the similarities and differences that arise when oblique shock reflection is considered on cones, cylinders, and spheres relative to the well-studied case of a planar wedge using past theoretical, experimental and numerical results.

## 1 Introduction and Scope

Oblique shock interactions with solid surfaces have been a research area of interest since 1878, when Mach experimentally discovered the basic three-shock Mach reflection pattern [1]. Since then, significant efforts have been made theoretically, experimentally, and numerically to better understand the underlying physics of oblique shock interaction. Examples of notable experimental studies include the work by Skews [2], Ben-Dor [3], and Takayama et al. [4]. With the advent of everincreasing computing power and the availability of high-performance computing (HPC) resources, computational fluid dynamics (CFD) has become a powerful tool in this area of study. Attempts to study the oblique shock interaction problem from a numerical standpoint include contributions from researchers such as Glaz et al. [5, 6], Collela and Henderson [7], Timofeev et al. [8], Drikakis et al. [9], Saito et al. [10], and Hryniewicki et al. [11–13].

One of the key areas of study concerning oblique shock interaction is that of the transition from regular reflection (RR) to Mach reflection (MR); a phenomena in

M. Grzeszczyk ( $\boxtimes$ ) · J. J. Gottlieb · C. P. T. Groth University of Toronto Institute for Aerospace Studies, Toronto, Canada e-mail: marcel.grzeszczyk@mail.utoronto.ca

<sup>©</sup> The Author(s), under exclusive license to Springer Nature Singapore Pte Ltd. 2025 R. S. Myong and H. D. Kim (eds.), *Proceedings of the 34th International Symposium on Shock Waves, Volume 1: Fundamentals*, https://doi.org/10.1007/978-981-96-4767-5\_28

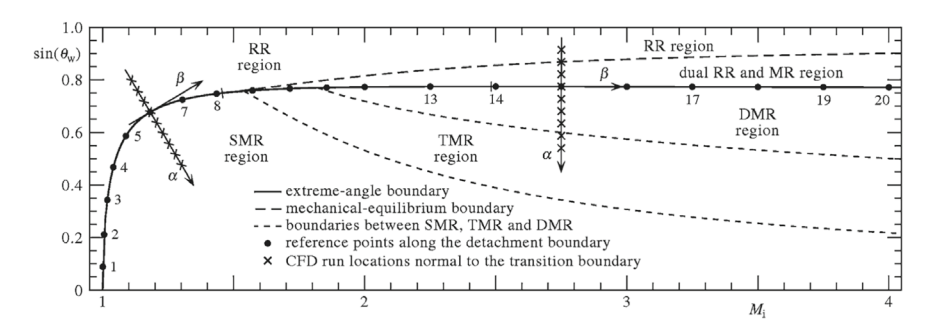


**Fig. 1** Regions of regular and Mach reflection for an inviscid polytropic air flow past a wedge separated by the analytical transition boundaries. Also shown are the reference points,  $RP - i = (M_i^*, \theta_w^*)$ , along the extreme-angle boundary between RR and MR defined by Hryniewicki et al. [12] and the local  $(\alpha, \beta)$ -coordinate system defined at each of these points defining the coordinates normal and tangent to the boundary

which a two-shock RR configuration transitions into a three-shock MR configuration on the reflecting surface. The RR-MR transition criteria is dependent on the geometry of the reflecting surface. A wide range of literature exists concerning the RR-MR transition on a planar wedge since the 1940s, with experimental and theoretical contributions from researchers such as von Neumann [14], Bleakney and Taub [15], Courant and Friedrichs [16], Henderson and Lozzi [17], and Ben-Dor and Glass [18, 19].

In the present study, the transition from RR to MR for non-stationary oblique shock interactions with various canonical two-dimensional geometries, including wedges (ramps), cones, semicylinders, and semi-spheres in inviscid, polytropic air is further examined in a systematic fashion via numerical methods. Moreover, the similarities and differences that arise when oblique shock reflection is considered on cones, cylinders, and spheres relative to the more well-studied case of a planar wedge are examined with the aid of new simulation results and past theoretical and experimental results.

## 2 Approach for Detection of RR-MR Transition

The theoretical boundaries that define the RR-MR transition on planar ramps or wedges are the extreme-angle (detachment), the sonic, and mechanical-equilibrium boundaries as identified by von Neumann [12–14]. These boundaries separate the four classes of reflection phenomena possible on wedges, cones, cylinders, and spheres: regular reflection, single Mach reflection (SMR), transitional Mach reflection (TMR), and double Mach reflection (DMR). The extreme-angle and mechanical-equilibrium boundaries that separate these reflection regimes are shown as a function of the wedge angle,  $\theta_{\rm w}$ , and incident shock Mach number,  $M_{\rm i}$ , in Fig. 1 for oblique shock reflection

in inviscid polytropic air. Note that the sonic boundary (not shown) lies very close to the extreme-angle boundary.

When the oblique shock reflection problem is considered on a cylinder, it can be thought of as an equivalent problem to that of a time-variant wedge, where the wedge angle changes as a function of time [20]. The equivalent wedge angle for a cylinder is linked to the position of the incident shock on the cylinder surface. The leading edge of the cylinder corresponds to a upward-facing wall with a wedge angle of  $\theta_{\rm w}=90^{\circ}$  ( $\pi/2$  radians) and the cylinder apex corresponds to an equivalent wedge angle of  $\theta_{\rm w}=0^{\circ}$ . The angular position,  $\omega$ , of the incident shock on the cylindrical surface of radius, R, measured clockwise from the leading edge, is related to the equivalent wedge angle through the following relationship:

$$\theta_{\rm w} = \frac{\pi}{2} - \omega,\tag{1}$$

where

$$x = R - R\cos(\omega), \quad y = R\sin(\omega),$$
 (2)

describe the position of the incident shock in terms of coordinates, (x, y), of the twodimensional Cartesian frame. These relationships can also be applied in the case of a sphere, which acts as an axisymmetric variant of the cylinder, where here the ycoordinate is taken to be radial coordinate direction.

For studies involving the RR-MR transition on the wedge and cone geometries, multiple numerical simulations are conducted at conditions clustered about reference points of interest corresponding to the extreme-angle boundary. The 20 reference points, RP- $i = (M_i^*, \theta_w^*)$ , defined along the extreme-angle boundary by Hryniewicki et al. [12] are depicted in Fig. 1. For each numerical simulation, the incident shock Mach number and wedge angle are varied using an  $(\alpha, \beta)$ -coordinate transformation [13] in which

$$M_{\rm i} = M_{\rm i}^* + \alpha \cos(\phi^*) - \beta \sin(\phi^*), \qquad (3)$$

$$\sin(\theta_{\rm w}) = \sin(\theta_{\rm w}^*) + \alpha \sin(\phi^*) + \beta \cos(\phi^*), \tag{4}$$

$$\phi^* = \tan^{-1} \left( \frac{\mathrm{d} \sin(\theta_{\mathrm{w}})}{\mathrm{d} M_{\mathrm{i}}} \Big|_* \right) - 90^{\circ} \,, \tag{5}$$

where  $(M_i^*, \theta_w^*)$  are the incident shock Mach number and wedge angle corresponding to the reference point of interest and  $\operatorname{d} \sin(\theta_w)/\operatorname{d} M_i|_*$  is the slope of the extreme-angle boundary at the reference point of interest. In the axisymmetric case of a cone,  $\theta_w$  corresponds to the cone half-angle. Each  $(M_i, \theta_w)$  test pair is generated by varying  $\alpha$  and setting  $\beta=0$ , which ensures traversal normal to the extreme-angle boundary, wherein  $\alpha<0$  tests points located above the boundary and  $\alpha>0$  tests points below the boundary. For each value of  $\alpha$  tested, a non-dimensional parameter L is computed, which represents the separation distance between the incident shock and Mach stem. L is defined as:

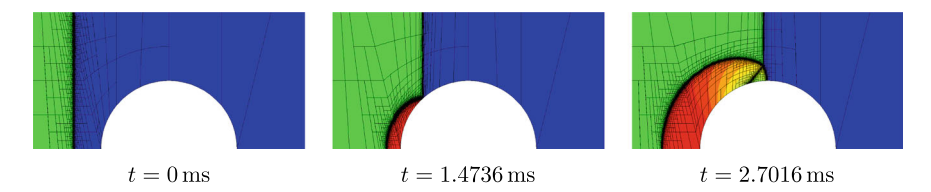


**Fig. 2** Predicted distributions of the flow density for the interaction of a normal shock of strength  $M_i = 1.43$  with a semicircular cylinder. Flow solutions are shown before interaction (left), during regular reflection (middle), and after transition to Mach reflection (right) on the cylinder

$$L = \frac{z_{c,1} - z_{c,u}}{z_{c,u}},$$
 (6)

where  $z_{\rm c,l}$  is the distance travelled by center of the shock attached to the reflection surface, and  $z_{\rm c,u}$  is the distance travelled by the center of the shock attached to the far-field top boundary of the computational grid. In the case of a regular reflection, both  $z_{\rm c,l}$  and  $z_{\rm c,u}$  correspond to the distance travelled by the incident shock, which should cause L to vanish. In the case of a Mach reflection, the Mach stem will remain attached to the reflection surface and travels at a higher speed than the incident shock, which results in the difference  $z_{\rm c,l}-z_{\rm c,u}$  representing the difference in distance travelled by the Mach stem and incident shock. This difference is normalized by  $z_{\rm c,u}$  due to the fact that these reflection patterns grow in size over time. The point at which L vanishes corresponds to the RR-MR transition.

A somewhat analogous procedure is adopted herein for determining the RR-MR transition on the cylinder and sphere, wherein the distances travelled by the center of the shock fronts attached to the top far-field boundary and cylinder reflection surface are tracked and compared via the difference  $\Delta z = z_{\rm c,l} - z_{\rm c,u}$ . Unlike the case of a wedge, where multiple numerical simulations are necessary to capture a sweep of  $\theta_{\rm w}$  values for a given test value of  $M_{\rm i}$ , a continuous sweep of wedge angles are automatically tested as the incident shock propagates over the cylinder; therefore, only requiring variation in  $M_i$  for cylinder simulations. When the incident shock first makes contact with the leading edge of the cylinder, the resultant reflection pattern that emerges will always start as a regular reflection, however, as the cylinder is convex and  $\theta_{\rm w}$  decreases as the incident shock traverses over the cylinder, the resultant reflection pattern will eventually change into a Mach reflection. An example of this unsteady transition behaviour is shown in Fig. 2. When the reflection pattern remains regular,  $\Delta z = 0$ ; when the reflection pattern transitions into Mach reflection  $\Delta z > 0$ and will continue to grow. The equivalent wedge angle on the cylinder that causes  $\Delta z$  to grow denotes the RR-MR transition on the cylinder. The RR-MR transition for an axisymmetric sphere is similar to that for the planar cylinder.

## 3 Numerical Method for Unsteady Oblique Shock Reflections

#### 3.1 Governing Equations

In this numerical study, two-dimensional planar and axisymmetric inviscid shock reflection processes are considered. Accordingly, numerical solutions of the Euler equations governing two-dimensional, compressible, gaseous flows associated with planar Cartesian and axisymmetric coordinate systems are examined. The Euler equations in this case can be summarized in matrix-vector form as

$$\frac{\partial \mathbf{U}}{\partial t} + \vec{\nabla} \cdot \vec{\mathbf{F}} = \frac{\partial \mathbf{U}}{\partial t} + \frac{\partial \mathbf{F}}{\partial x} + \frac{\partial \mathbf{G}}{\partial y} = \mathbf{S}_{a},\tag{7}$$

where t is the physical time, x and y are the two spatial coordinates,  $\mathbf{U}$  is the conserved solution column vector, and  $\mathbf{F}$  and  $\mathbf{G}$  are the inviscid solution flux column vectors in the x- and y-coordinate directions, respectively,  $\vec{\mathbf{F}} = [\mathbf{F}, \mathbf{G}]$  is the two-dimensional solution flux dyad, and  $\mathbf{S}_a$  is a source term column vector associated with axisymmetric geometry. In Eq. (7),  $\mathbf{U}$ ,  $\mathbf{F}$  and  $\mathbf{G}$  have the form

$$\mathbf{U} = \begin{bmatrix} \rho \\ \rho u \\ \rho v \\ \rho E \end{bmatrix}, \ \mathbf{F} = \begin{bmatrix} \rho u \\ \rho u^2 + p \\ \rho u v \\ \rho u \left( E + \frac{p}{\rho} \right) \end{bmatrix}, \ \mathbf{G} = \begin{bmatrix} \rho v \\ \rho u v \\ \rho v^2 + p \\ \rho v \left( E + \frac{p}{\rho} \right) \end{bmatrix}, \tag{8}$$

where  $\rho$  is the flow density, u and v are the flow velocity components in the x- and y-coordinate directions, respectively, p is the pressure, and  $E = e + (u^2 + v^2)/2$  is the total specific energy of the gas expressed in terms of the specific internal energy, e, and the specific kinetic energy. Additionally, for planar geometry,  $\mathbf{S}_a = \mathbf{0}$ , and, for axisymmetric geometry,

$$\mathbf{S}_{\mathbf{a}} = -\frac{1}{y} \left[ \rho v, \rho u v, \rho v^2, \rho v \left( e + \frac{p}{\rho} \right) \right]^{\mathsf{T}}. \tag{9}$$

# 3.2 Upwind Finite-Volume Method

A high-resolution, upwind, Godunov-type, finite-volume method [21] is used in the spatial discretization of the Euler equations given previously in Eq. (7). As described in more detail by Hryniewicki et al. [22], the integral form of Eq. (7) is solved on quadrilateral-shaped computational cells or elements, (i, j), of two-dimensional, multi-block, body-fitted, computational meshes as illustrated in Fig. 3a, having cen-

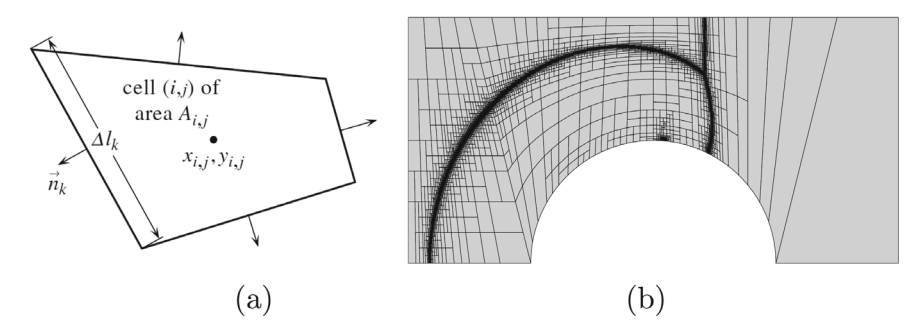


Fig. 3 Illustration of two-dimensional multi-block body-fitted mesh used in finite-volume discretization showing (a) the quadrilateral cell (element) and (b) an example multi-block anisotropic AMR mesh with 11 levels of mesh refinement consisting of 17,995  $8 \times 8$  grid blocks (boundaries of grid blocks are shown) for a total of 1,151,680 quadrilateral cells

troid,  $(x_{i,j}, y_{i,j})$ , area,  $A_{i,j}$ , four cell faces, k, with face lengths,  $\Delta \ell_{i,j,k}$ , and outward-pointing, face-normal, unit vectors,  $\vec{n}_{i,j,k}$ , for k = 1, 2, 3, 4. Following application of the divergence theorem and a second-order accurate, mid-point, quadrature rule for the evalution of the closed-path integral of the flux on the faces of the quadrilateral cell, the following semi-discrete form of Eq. (7) is obtained

$$\frac{d\mathbf{\tilde{N}}_{i,j}}{dt} = -\frac{1}{A_{i,j}} \sum_{k=1}^{4} \left( \vec{\mathbf{F}} \cdot \vec{n} \,\Delta \ell \right)_{i,j,k} + \mathbf{S}_{a,i,j} = \mathbf{R}_{i,j}(\mathbf{U}), \tag{10}$$

where  $\mathbf{v}_{i,j} = (1/A) \int_A \mathbf{U}_{i,j} dA$  is the cell-averaged conserved solution vector and  $\mathbf{R}_{i,j}$  is the solution residual. The values of the inviscid flux vector,  $\vec{\mathbf{F}}$ , on the cell boundary is evaluated herein by using a combination of a Riemann-solver-based flux function and second-order, piecewise linear, limited reconstruction. In particular, the approximate Riemann solver of Harten, Lax, and van Leer [23], with the evaluation of the wave speeds as suggested by Einfeldt [24], are used. Piecewise linear reconstruction of the primitive solution quantities,  $\rho$ , u, v, and p, within each cell is carried out as described by Barth [25] and the slope limiter of Venkatakrishnan [26] is used, to ensure solution monotonicity in the presence of discontinuous solutions and shocks.

A conditionally-stable, explicit, two-stage, Runge-Kutta (RK2), time-marching scheme is used to integrate the semi-discrete form of the Euler equations given by Eq. (10). For an appropriately restrictive choice of physical time step,  $\Delta t$ , satisfying a Courant-Friedrichs-Lewy (CFL) condition, the latter can be shown to be strong stability preserving (SSP) when applied along with the limited, upwind, finite-volume scheme outlined above as originally described by Shu and Osher [27, 28]. The SSP property ensures accurate and positive treatment of unsteady solution content associated with discontinuities and shocks.

### 3.3 Anisotropic Block-Based Adaptive Mesh Refinement

As indicated above, the proposed finite-volume discretization of the governing partial differential equations has been implemented for quadrilateral elements which are contained within structured grid blocks of a multi-block, body-fitted, computational grid. See Fig. 3(b). In order to ensure accurate and high-resolution treatment of the unsteady shock reflection flows of interest, an anisotropic block-based adaptive mesh refinement (AMR) method, based on the previous work of Williamschen and Groth [29], Freret and Groth [30], and Freret et al. [31] and as implemented by Hryniewicki et al. [22], is also used here. In the block-based anisotropic AMR approach, the two-dimensional grid blocks of the multi-block mesh are automatically coarsened or refined, depending on the solution, in a preferred coordinate direction in order to handle flows with strong anisotropic solution features, as demonstrated in Fig. 3(b). Grid block refinement is performed periodically at regular intervals during the simulation based on local spatial gradients of the flow density and flow velocity magnitude [29-31]. The computational advantage of the current AMR strategy is the ability to refine locally the computational mesh as the solution evolves in time, with the refinement occurring only in regions of interest to the study, such as a shock front, while leaving the grid in less important flow regions relatively coarse.

#### 4 Numerical Results

The numerically-determined RR-MR transition points are now considered for the cases of a normal shock in air interacting with two-dimensional smooth wedges, cones, semicircular cylinders, and spheres. Transition results for each of these geometries are shown for incident shock strengths of  $M_i = 1.305$  and  $M_i = 3.00$ , corresponding to reference points RP-07 = (1.305, 46.4516°) and RP-16 = (3.00, 50.703°) on the extreme-angle boundary. For each case considered, the numerically-determined RR-MR transition points are compared to the corresponding extreme-angle and sonic boundary values for wedges.

# 4.1 RR-MR Transition for Wedges and Cones

The RR-MR transitions are depicted as a function of  $\alpha$  in Fig. 4 for reference points RP-07 and RP-16 based on numerous simulations of the non-stationary shock reflection process for the wedge (each point of the curve corresponds to a full simulation), where the parameter, L, is the non-dimensional representation of the Mach stem separation distance defined earlier. Simulation results are shown for three different levels of AMR (13, 14, and 15) allowing the grid convergence of the predicted transitions to be assessed. An increase in the level of refinement by one provides a reduction

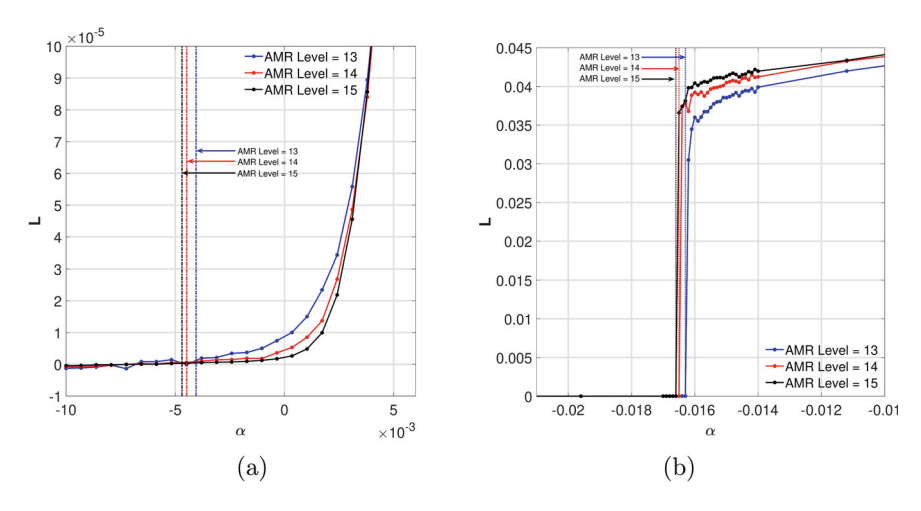


**Fig. 4** Predicted RR-MR transition in  $(L, \alpha)$ -space for non-stationary shock reflection processes on a wedge corresponding to (a) reference points RP-07 =  $(1.305, 46.4516^{\circ})$  and (b) RP-16 =  $(3.00, 50.703^{\circ})$ , respectively, obtained using 13, 14, and 15 levels of anisotropic AMR

**Table 1** Summary of numerically-determined RR-MR transition points for inviscid air flow past a wedge and cone with comparisons to values for the extreme-angle and sonic boundaries for wedges. Wedge results are denoted with W; cone results are denoted with C

RP	Extreme-Angle Sonic			Ref. [12]	Current Wedge & Cone Results				
	$M_{\rm i}^*$	θ <sub>w</sub> (°)	θ <sub>w</sub> (°)	θ <sub>w</sub> (°)	$M_{\rm i}$	$\Delta M_{\rm i}$	θ <sub>w</sub> (°)	$\Delta \theta_{ m W}$ (°)	
7	1.305	46.452	46.835	46.460	1.304	±0.001	46.83	±0.02	W
					1.304	±0.001	46.85	±0.02	C
16	3.000	50.703	50.812	52.137	3.000	$\pm 0.0001$	52.23	$\pm 0.01$	W
					3.000	$\pm 0.0001$	52.19	±0.01	С

in the minimum mesh spacing by a factor of two and the finest AMR grid (level 15) involved minimum mesh spacings that were a factor of four times smaller than the level 13 mesh. For AMR level 15, the adapted meshes in the simulations generally contained between 4,000 and 6,000 8 × 8 grid blocks and ranged in size from 2,500,000 to nearly 4,000,000 computational cells. The ratio of the minimum mesh spacing to wedge length,  $\Delta x_{\min}/L_{\rm w}$ , for the anisotropic AMR meshes with 13, 14, and 15 levels of refinement were  $4.97 \times 10^{-5}$ ,  $2.48 \times 10^{-5}$ ,  $1.24 \times 10^{-5}$ , respectively, with  $L_{\rm w}=1$  m. Each simulation was initialized with a normal shock placed 40 cm away from the wedge/cone surface, with flow conditions downstream of the shock corresponding to atmospheric conditions ( $p_1=101.325$  kPa,  $T_1=295.0$  K,  $\rho_1=1.197$  kg/m³). Flow conditions upstream of the incident shock were calculated using the Rankine-Hugoniot jump conditions. Reflection boundary conditions were used for the wedge and cone surface as well as the far-field top boundary of the computational grid.

For reference point RP-07, which is associated with RR-MR transition at shock Mach numbers below the dual region, there is continuous and gradual increase in L with  $\alpha$  and transition is taken to occur when L>0. The estimates of the transition point are represented in Fig. 4(a) by the three vertical lines for the anisotropic AMR meshes with 13, 14, and 15 levels of refinement. It is evident that there is convergence of the predicted transition location as the mesh is refined. For reference point RP-16, which lies within the so-called dual region, the value of L remains zero up until there is a sudden and discontinuous change in L, after which L remains positive valued and continues to gradually increase. The location for the discontinuous change in L is taken to be the point for RR-MR transition and is represented in Fig. 4(b) by the three vertical lines for AMR mesh refinement levels 13, 14, and 15. Again, convergence of the predicted transition point is evident as the mesh is refined. A similar set of results for RR-MR transition in air were also obtained for axisymmetric cones at RP-07 and RP-16 but are not shown.

Summaries of the RR-MR transition results for the wedge and cone are provided in Table 1, as well as graphically in Fig. 5, for reference points RP-07 and RP-16. The values reported here are based on the AMR mesh simulations with 15 levels of refinement and a Richardson extrapolation procedure assuming first-order convergence (due to limiting in finite-volume solutions) was used to estimate the errors in the transition incident Mach number and angle,  $\Delta M_i$  and  $\Delta \theta_w$ , respectively. It can be seen that the current predictions of the transitions for the wedge and cone at reference points RP-07 and RP-16 are nearly equal, with differences in the transition wedge angle on the order of the estimated numerical error. This is not unexpected. Furthermore, when these numerically-determined RR-MR transition points are compared to the extreme-angle and sonic boundaries, it is evident that, for point RP-07 outside the dual region, the predicted transition points are in excellent agreement with both inviscid theoretical results. Closer agreement to the sonic condition can be observed. However, for point RP-16, which lies within the dual region in terms of Mach number, the predicted RR-MR transition is located above the extreme-angle and sonic boundaries and is found to occur fully within the dual-region. Note that these findings are fully consistent with the previous numerically-determined RR-MR transition for wedges of Hryniewicki et al. [12], although the predicted transition points are estimated to occur at very slightly larger wedge angles than those reported in this previous study.

# 4.2 RR-MR Transition for Cylinders and Spheres

The computed RR-MR transition for non-stationary shock reflection processes on a semicylinder at reference points RP-07 and RP-16 based on a single unsteady numerical simulation is given in Fig. 6. As for the wedge and cone predictions, simulation results are shown for three different levels of AMR (10, 11, and 12). The finest adapted anisotropic AMR meshes consisted of between 1,300 to 2,000  $8 \times 8$  grid blocks and approximately 900,000 to 1,200,000 computational cells. In these

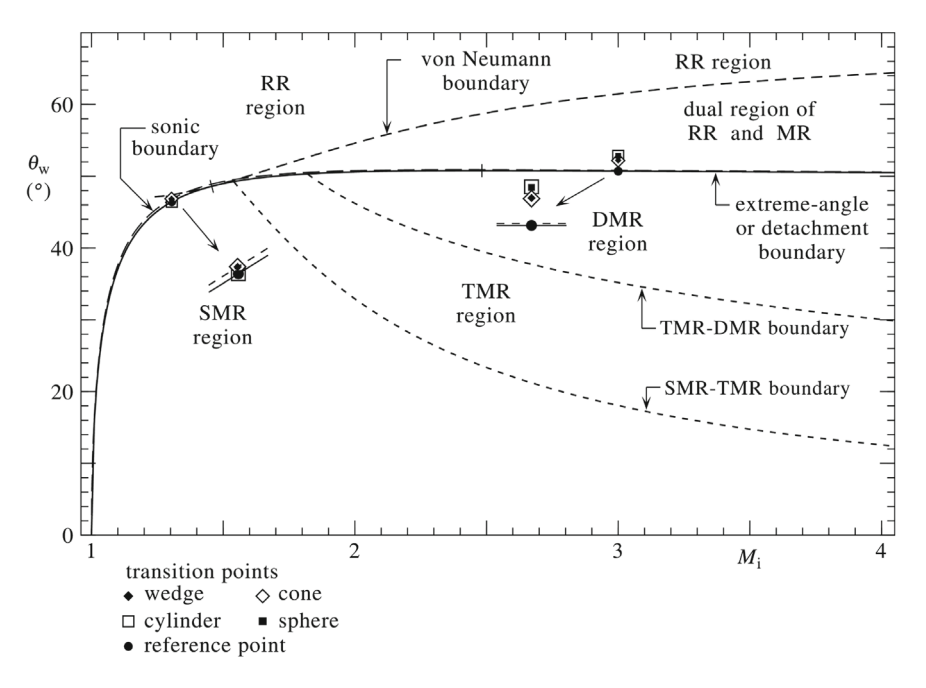


**Fig. 5** Regions of regular and Mach reflection for in inviscid polytropic air flow past a wedge separated by the analytical transition boundaries showing current numerical predictions of the equivalent RR-MR transition for wedges, cones, cylinders, and spheres for reference points RP-07 and RP-16

cases, the ratio of the minimum mesh spacing to radius of the cylinder,  $\Delta x_{\rm min}/R$ , for the anisotropic AMR meshes with 10, 11, and 12 levels of refinement were  $1.26 \times 10^{-4}, 6.28 \times 10^{-5}, 3.14 \times 10^{-5}$ , respectively, with R=1 m. The same initial conditions used for the wedge and cone geometries were used in these simulations. Similarly, reflection boundary conditions were used for the cylinder/sphere and top far-field boundary of the computational grid. For the cylindrical reflection geometry, the RR-MR transitions are depicted as a function of x/R in Fig. 6 for reference points RP-07 and RP-16. In the figure,  $\Delta z/R$  is given as a function of x/R and, as described previously, transition has occurred and a Mach reflection pattern has been established for  $\Delta z > 0$ . The estimated transition points are shown in the figure for the sequence of refined meshes. A similar set of computational results were obtained for the sphere but are not shown.

Summaries of the RR-MR transition results for the cylinder and sphere are provided in Table 2 and Fig. 5 for reference points RP-07 and RP-16. Richardson extrapolation was again used to estimate the error in the equivalent wedge angle,  $\Delta\theta_w$ , for the transitions. It is evident that, as for the wedge and cone results, the equivalent transition wedge angles for both the cylinder and sphere are equal to within the estimated numerical error. Furthermore, the numerically-determined transition points

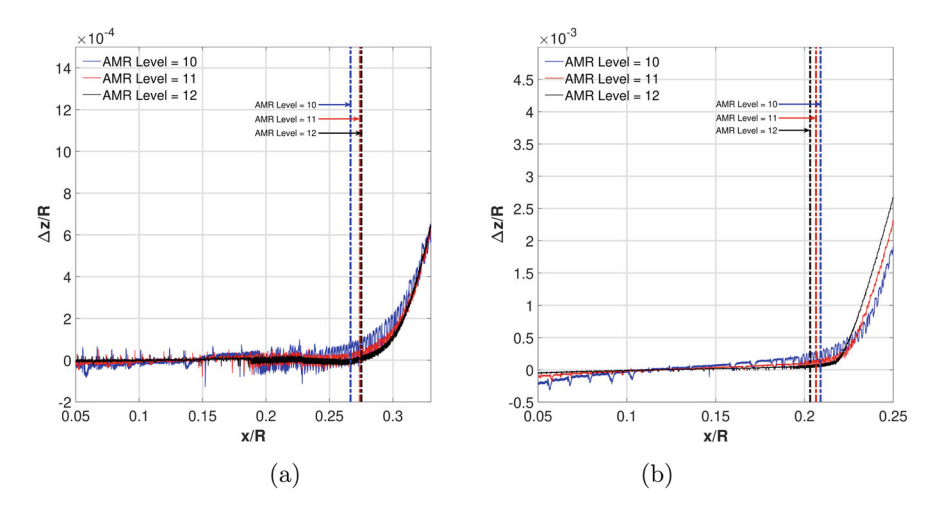


**Fig. 6** Predicted RR-MR transition in  $(\Delta z/R, x/R)$ -space for non-stationary shock reflection processes on a semicylinder corresponding to (a) reference points RP-07 =  $(1.305, 46.4516^{\circ})$  and (b) RP-16 =  $(3.00, 50.703^{\circ})$ , respectively, obtained using 10, 11, and 12 levels of anisotropic AMR

**Table 2** Summary of the numerically-determined RR-MR transition points for inviscid air flow past a cylinder and sphere with comparisons to values for the extreme-angle and sonic boundaries for wedges

RP	Extreme-angle		Sonic	Ref. [12]	Cylinder		Sphere	
	$M_{\rm i}^*$	θ* (°)	θ <sub>w</sub> (°)	θ <sub>w</sub> (°)	θ <sub>w</sub> (°)	$\Delta \theta_{ m w}$ (°)	θ <sub>w</sub> (°)	$\Delta \theta_{ m w}$ (°)
7	1.305	46.452	46.835	46.460	46.454	±0.10	46.47	±0.30
16	3.000	50.703	50.812	52.137	52.83	±0.30	52.852	±0.25

for RP-07 and RP-16 are in full agreement with the wedge and cone results of the previous section.

#### 5 Conclusions

In this study, the RR-MR transition was examined for the case of a normal shock wave interacting with two-dimensional wedges, cones, cylinders, and spheres for inviscid air. A numerical methodology to accurately determine the RR-MR transition points for all of these canonical geometries was presented. The proposed approach makes use of a systematic post-processing methodology applied to the numerical solutions of the Euler equations, which were obtained through the use of high-fidelity CFD based on a combination of an accurate and robust upwind finite-volume scheme and anisotropic block-based AMR strategy. The latter permitted the convergence of the numerical predictions and error to be demonstrated. The present results for the

various geometries confirm the previous numerically-determined RR-MR transition results on wedges alone obtained in previous studies by Hryniewicki et al. [12] and Gottlieb et al. [13]. In particular, the transition predictions for all reflection geometries considered, including both planar and axisymmetric cases, were found to agree within the estimate computational error of the finite-volume solution method. Furthermore, the predicted transitions were found to occur at equivalent wedge angles with values considerably above the extreme-angle and sonic boundaries and located fully inside the dual-region at higher Mach numbers. Future follow-on studies will consider RR-MR transitions at other reference points along the extreme-angle boundary, both outside and within the dual region, as well as the important influence of viscous effects on transitions from regular to Mach reflection.

**Acknowledgements** The computational resources for performing the numerical simulations reported herein were provided by the SciNet High Performance Computing Consortium at the University of Toronto and the Digital Research Alliance of Canada.

#### References

- Mach, E.: Uber den Verlauf der Funkenwellen in der Ebene und im Raum. Sitzungsbr Akad Wien 78, 819–838 (1878)
- Skews, B.W.: The perturbed region behind a diffracting shock wave. J. Fluid Mech. 29(4), 705–719 (1967)
- 3. Ben-Dor, G.: Shock Wave Reflection Phenomena. Springer-Verlag, Berlin (1991)
- 4. Takayama, K., Kleine, H., Grönig, H.: An experimental investigation of the stability of converging cylindrical shock waves in air. Exp. Fluids 5(5), 315–322 (1987)
- Glaz, H.M., Colella, P., Glass, I.I., Deschambault, R.L.: A numerical study of oblique shockwave reflections with experimental comparisons. Proc. Royal Soc. London A 398, 117–140 (1985)
- Glaz, H. M., Colella, P., Glass, I.I., Deschambault, R.L.: Report 285. Institute for Aerospace Studies, University of Toronto (1986)
- Colella, P., Henderson, L.F.: The von Neumann paradox for the diffraction of weak shock waves. J. Fluid Mech. 213, 71–94 (1990)
- 8. Timofeev, E., Takayama, K., Voinovich, P.: Paper 97-0070, AIAA (1997)
- Drikakis, D., Ofengeim, D., Timofeev, E., Voionovich, P.: Computation of non-stationary shock-wave/cylinder interaction using adaptive-grid methods. J. Fluids Struct 11(6), 665–692 (1997)
- 10. Saito, T., Voinovich, P., Timofeev, E., Takayama, K.: In: Toro, E.F. (ed.) Godunov Methods: Theory and Applications, pp. 763–784. Springer, Boston (2001)
- 11. Hryniewicki, M.K.: On the transition boundary between regular and Mach reflections from a wedge in inviscid and polytropic gases. Ph.D. thesis, University of Toronto (2016)
- 12. Hryniewicki, M.K., Gottlieb, J.J., Groth, C.P.T.: Transition boundary between regular and mach reflections for a moving shock interacting with a wedge in inviscid and polytropic air. Shock Waves 27(4), 523–550 (2017)
- Gottlieb, J.J., Hryniewicki, M.K., Groth, C.P.T.: Transition boundary between regular and mach reflections for a moving shock interacting with a wedge in inviscid and polytropic argon. Shock Waves 29(6), 795–816 (2019)
- 14. von Neumann, J.: Explosives Research Report No. PB37079. U.S. Bureau of Ordinance (1943)

- 15. Bleakney, W., Taub, A.H.: Interaction of shock waves. Rev. Modern Phys. 21(4), 584–605 (1949)
- Courant, R., Friedrichs, K.O.: Supersonic Flow and Shock Waves, 5th edn. Springer, New York (1999)
- Henderson, L.F., Lozzi, A.: Experiments on transition of mach reflection. J. Fluid Mech. 68, 139–155 (1975)
- 18. Ben-Dor, G., Glass, I.I.: Domains and boundaries of non-stationary oblique shock-wave reflexions. 1. Diatomic gas. J. Fluid Mech. **92**, 459–496 (1979)
- 19. Ben-Dor, G., Glass, I.I.: Domains and boundaries of non-stationary oblique shock-wave reflexions. 2. Monatomic gas. J. Fluid Mech. **96**, 735–756 (1980)
- 20. Kaca, J.: Technical Note 269. University of Toronto Institute for Aerospace Studies (1988)
- 21. Godunov, S.K.: Finite-difference method for numerical computations of discontinuous solutions of the equations of fluid dynamics. Mat. Sb. 47, 271–306 (1959)
- 22. Hryniewicki, M.K., Groth, C.P.T., Gottlieb, J.J.: Parallel implicit anisotropic block-based adaptive mesh refinement finite-volume scheme for the study of fully resolved oblique shock wave reflections. Shock Waves **25**(4), 371–386 (2015)
- Harten, A., Lax, P.D., van Leer, B.: ] On upstream differencing and Godunov-type schemes for hyperbolic conservation laws. SIAM Rev. 25(1), 35–61 (1983)
- Einfeldt, B.: On Godunov-Type methods for gas dynamics. SIAM J. Numer. Anal. 25, 294–318 (1988)
- 25. Barth, T.J.: Paper 93-0668, AIAA (1993)
- 26. Venkatakrishnan, V. Paper 93-0880, AIAA (1993)
- Shu, C.-W., Osher, S.: Efficient implementation of essentially non-oscillatory shock-capturing schemes. J. Comput. Phys. 77, 439–471 (1988)
- 28. Gottlieb, S., Shu, C.-W., Tadmor, E.: Strong stability-preserving high-order time discretization methods. SIAM Rev. **43**(1), 89–112 (2001)
- 29. Williamschen, M.J., Groth, C.P.T. Paper 2013-2442, AIAA (2013)
- 30. Freret, L., Groth, C.P.T.: Paper 2015-2613, AIAA (2015)
- 31. Freret, L., Williamschen, M., Groth, C.P.T.: Enhanced anisotropic block-based adaptive mesh refinement for three-dimensional inviscid and viscous compressible flows. J. Comput. Phys. **458**, 111092 (2022)